Sag in Commercial Thermoforming

H. M. Baek
Rheology Research Center, Mechanical Engineering Dept., University of Wisconsin-Madison, Madison, WI 53706

A. J. Giacomin
Chemical Engineering Dept., Queen's University, Kingston, ON, Canada K7L 3N6

M. J. Wurz
Sub-Zero, Inc., Madison, WI 53711

DOI 10.1002/aic.14275
Published online November 21, 2013 in Wiley Online Library (wileyonlinelibrary.com)

Our previous analytical solution gives sag advancing implicitly as $\Theta=\frac{1}{2}\left[\arctan\Sigma-\left\{\Sigma/\left(\Sigma^2+1\right)\right\}\right]$, *or for* $\Sigma\leq\frac{2}{5}$, *sag advances with the cube root of time for a thin wide rectangular Newtonian isothermal sheet. This previous analytical work applies to sheets that are pinned along just two edges, and not all the way around. Corresponding sagometer experimental results confirmed this cube root relation. This work compares the* $\Theta=\frac{1}{2}\left[\arctan\Sigma-\left\{\Sigma/\left(\Sigma^2+1\right)\right\}\right]$ *prediction with measured commercial thermoforming behavior on rectangular sheets that are, of course, pinned all the way around. Then sag parallel superposition is used to extend* $\Theta=\frac{1}{2}\left[\arctan\Sigma-\left\{\Sigma/\left(\Sigma^2+1\right)\right\}\right]$ *for a sheet pinned all the way around. We evaluate sag parallel superposition using a finite element method (FEM) employing ANSYS Polyflow. The equation* $\Theta=\frac{1}{2}\left[\arctan\Sigma-\left\{\Sigma/\left(\Sigma^2+1\right)\right\}\right]$ *assumes sagging sheet cylindricity, and from our FEM we find that this assumption is reliable when* $\Sigma\leq\frac{3}{2}$. *We compare sag measured in commercial thermoforming, using high-impact polystyrene (HIPS) sheets that are pinned all the way around, by extending* $\Theta=\frac{1}{2}\left[\arctan\Sigma-\left\{\Sigma/\left(\Sigma^2+1\right)\right\}\right]$ *with parallel superposition. It is found that the time evolution of the commercial sag follows nearly exactly the same shape as the isothermal prediction. We measure sag runaway, and although the isothermal analysis* $\Theta=\frac{1}{2}\left[\arctan\Sigma-\left\{\Sigma/\left(\Sigma^2+1\right)\right\}\right]$, *predicts the sag runaway time accurately, our isothermal theory overpredicts the amount of sag in the nonisothermal commercial operation by as much as a factor of 14. It is also shown how to use sheet sag measurements from commercial thermoforming to deduce the Newtonian viscosity of a thermoforming resin at a temperature that is above its softening point.* © 2013 American Institute of Chemical Engineers *AIChE J*, 60: 1529–1535, 2014
Keywords: computational fluid dynamics (CFD), polymer processing, rheology

Introduction

A plastic sheet translates horizontally through an oven between two horizontal banks of radiative heaters. The solid sheet droops a little under its own weight giving it a little *initial sheet curvature*. Once softened, the melt plastic sheet descends under its own weight and we call this *sag*. This affects the position and orientation of each sheet element with respect to the heater bank,[1] causing variations in the heat flux distribution across the sheet, and, hence, complicating the subsequent shaping of the sheet.[2–7]* Understanding of the sheet's sag behavior for a given temperature and time helps thermoforming engineers choose their thermoforming processing parameters.

Stephenson[8] and Stephenson et al.[9] explored the role of viscoelasticity in thermoforming sag using the upper convected Maxwell model with the finite element method, for very low extensional rates ($\dot{\varepsilon}<0.01s^{-1}$). Sentmanat (see Eq. 16 of [10]) obtained an analytical solution for sag by modeling a sagging specimen as a classic beam deflecting under its own weight. Giacomin et al.[11†] had previously interpreted sag in terms of a gravity-driven melt flow, and employed a transport phenomenon approach in cylindrical coordinates to obtain an analytical solution for dimensionless sag with time for a thin Newtonian isothermal sheet pinned at just two edges.

Here, we compare Giacomin's analytical solution[11] to both experimental measurements and finite element calculations for a sagging HIPS sheet of various dimensions. For a rectangular sheet pinned all the way around, we use the sag parallel superposition to extend the analytical solution.

Figure 1 shows a two-dimensional (2-D) orthomorphic sketch of a sagging sheet during thermoforming. Table 1

Correspondence concerning this article should be addressed to A. J. Giacomin at giacomin@queensu.ca.

*Errata: Eq. 13 should be $h/h_0\ll 1$; Eqs. 157, 165–169, 170 and 173–174 of Ref. 6 correct Eqs. 46, 53–57, 61 and 65–66, respectively; Table 1 of Ref. 6 corrects Table 1; Eqs. 152–153 of Ref. 6 correct Eqs. 32–33, in this connection, Figure 3 is in error.[2]

†Errata: After Eq. 24, "$\Theta_i=1$" should be "$\Theta_i=0.15$"; In the legends to Figures 7, 8 and 9, "Eq. 35" should be "Eq. 24".[11]

Table 1. Literature Cited on Sag in Thermoforming

Author (year)	Clamping	$\Sigma(t)$	$\Sigma < 0.2$	Material	Comment(s)	Reference
Cruz (1993)	*c*	○		PP	Rheological sag	18
Lucas (1995)				PP	Composition-dependent sag	19
Stephenson (1995, 1997, 1999)	*ee*			PS	Modeling sag using generalized Maxwell model	8,9,20
Lau et al. (1998, 2000)	*ee*	○		PP	Measurement of resistance to sag	21,22
Duarte and Covas (2002)	*ee*	○	○	PS	Modeling nonisothermal sag during heating	23
Debergue et al. (2004)					Modeling sag using K-BKZ model	24
Sentmanat (2004)					Rheological sag	10
Gupta and Misra (2006)	*ee*	○	○	ASA	Modeling sag using elastic, viscoelastic, hyperelastic models	25
Mohammadian-Gezaz et al. (2007)	*e*	○	○	PP	Formulation-dependent sag	26
Kershner and Giacomin (2007); Kershner (2007)	*ee*	○	○		Forming speed and sheet shape for conical mold	2,3
Lieg (2008); Lieg and Giacomin (2009)	*e*	○	○		Forming speed and sheet shape for molding a triangular trough	4,5
Giacomin et al. (2010)	*e*	○	○	PET, PP, HIPS	Analytical solution for sag using transport phenomena	11
Baek and Giacomin (2013); Baek (2013)	*ee*	○	○		Modeling sag using corotational and upper convected Maxwell models	6,7
This paper	*e*,*ee*	○	○	HIPS	Modeling commercial sag using isothermal theory	27

Legend: *ee* ≡ edges and ends; *e* ≡ edges only; c ≡ circular disk; ○ ≡ present

reviews the literature for analytical solutions for a sagging sheet. Table 2 lists dimensional variables and Table 3, the dimensionless ones.

Analytical Solution for Sag

Giacomin et al.[11] assumed that the sheet shape is nearly cylindrical when sagging, and, thus, modeled sag analytically for an infinitely long Newtonian isothermal sagging sheet that is pinned at just two opposing edges. They use cylindrical coordinates with descending origin (Figure 1). When pinned along the edges, the sheet follows a catenary and the droop. The corresponding physical intuition for the velocity profile is

$$\underline{v} = [v_r(r,t), 0, 0] \tag{1}$$

and the equation of continuity (see Eq. B.4–2 of [12]) simplifies to

$$\frac{\partial}{\partial r}(rv_r) = 0 \tag{2}$$

so that

$$rv_r = A(t) \tag{3}$$

The radial coordinate within the sheet r, is confined to

$$R \le r \le (R+\delta) \tag{4}$$

where δ is the sheet thickness, and R is the radius of sheet curvature. Eq. 4 can be adimensionalized to yield

$$1 \le \frac{r}{R} \le 1 + \frac{\delta}{R} \tag{5}$$

For a thin sheet

$$\frac{\delta}{R} \ll 1 \tag{6}$$

So Eq. 3 simplifies to

$$v_r \cong \frac{A(t)}{R} \tag{7}$$

For sag, a shearfree gravity-driven flow with Wi $\ll 1$ (see Table 3), we use the Newtonian constitutive equation for the equation of motion.[11] Using our physical intuition and neglecting fluid inertia, the r -component of the equation of motion (see Eq. B.6–4 of [12] or Eq. B.2–4 of [13]) yields

$$0 = \frac{-2v_r}{r^2} + \frac{\rho g}{\mu} \tag{8}$$

and for a thin sheet (Eq. 6)

$$0 = \frac{-2v_r}{R^2} + \frac{\rho g}{\mu} \tag{9}$$

which rearranges to

$$v_r = \frac{\rho g R^2}{2\mu} \tag{10}$$

Differentiating this yields

$$v_r = \frac{\mathrm{d}}{\mathrm{dt}}(d) \equiv d' = \frac{\rho g R^2}{2\mu} \tag{11}$$

which, from the trigonometry, can be rewritten as[14]

$$R \equiv \frac{r_0^2}{2d} + \frac{d}{2} \tag{12}$$

where r_0 is the half-width of the sagging sheet. Substituting Eq. 12 into Eq. 11 gives

$$\frac{d}{dt}(d) = \frac{\rho g}{2\mu}\left(\frac{r_0^2}{2d} + \frac{d}{2}\right)^2 \tag{13}$$

We adimensionalize Eq. 13 using Table 3 as

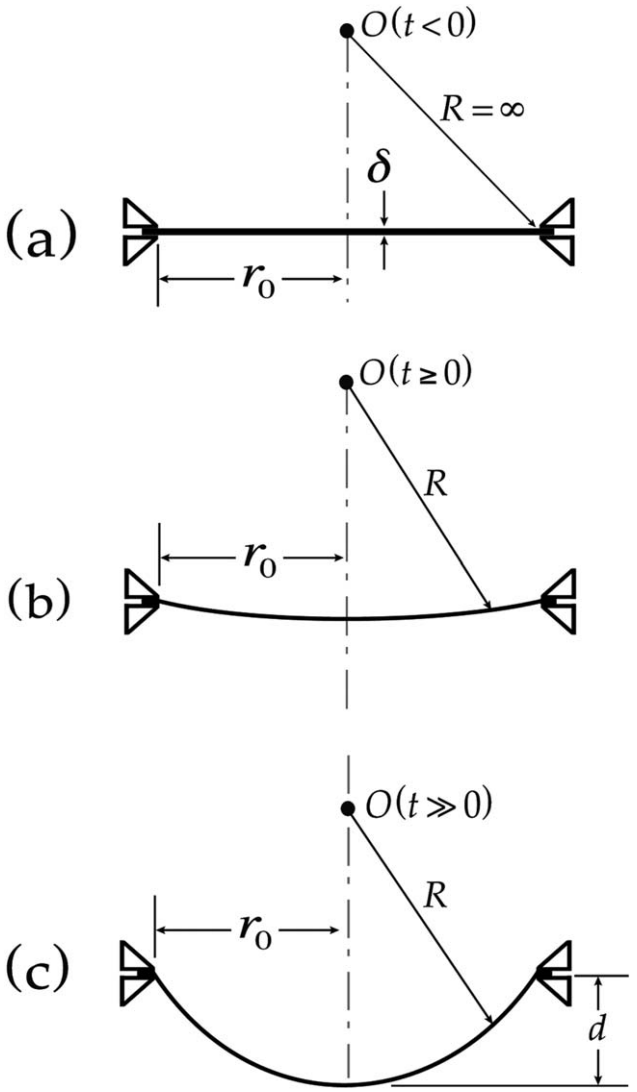

Figure 1. Two-dimensional orthomorphic sketch of thermoforming sheet with descending origin *O*(*t*), and pinned at just two edges (a) with no initial sheet curvature, (b) with little initial droop, and (c) sagging after softening.

Table 2. Dimensional Variables

Extensional rate	t^{-1}	$\dot{\varepsilon}$
Velocity	L/t	v
Newtonian viscosity	ML/t	μ
Newtonian viscosity at softening point	ML/t	μ_s
Gravity	M/t^2	g
Half sheet width	L	r_0
Density	M/L^3	ρ
Time	t	t
Relaxation time of fluid	t	λ
Vertical position	L	y
Sheet sag	L	d
Sheet sag in width direction	L	d_w
Sheet sag in length direction	L	d_ℓ
Total sheet sag of sheet pinned all the way around	L	d_t
Sheet thickness	L	δ
Sheet radius of curvature	L	R

Legend: M =; L = length; t = time; T = temperature

Table 3. Dimensionless Variables and Groups

Dimensionless sag	$\Sigma \equiv \frac{d}{r_0}$
Initial sag	Σ_0
Dimensionless time	$\Theta \equiv \frac{\rho g r_0}{8\mu} t$
Weissenberg number	$\mathrm{Wi} \equiv \lambda\dot{\varepsilon}$
Sag fitting parameter	ζ

$$\frac{d\Sigma}{d\Theta} = \left(\frac{1}{\Sigma} + \Sigma\right)^2 ; \Sigma \leq 1 \tag{14}$$

where the cylindricity assumption constrains the dimensionless sag to $\sum \leq 1$.

Without initial sheet curvature

If we neglect droop $d(0) = 0$, solving Eq. 14 without any initial sheet curvature $\sum_0 = 0$ yields the implicit expression

$$\Theta = \frac{1}{2}\left[\arctan(\Sigma) - \frac{\Sigma}{\Sigma^2+1}\right] \tag{15}$$

which is plotted in Figure 2. We find that sag first decelerates, inflects at $\Theta_i = 0.15$, and then eventually runs away at $\Theta_r = \pi/4$.[11] This appears to explain the sudden drop of the softened sheet onto the heater bank, an event Gupta and Misra call *catastrophic sag*.[11,25]

With initial sheet curvature

If we include droop $d(0) > 0$, solving Eq. 14 with an initial sheet curvature, $\sum_0$, yields

$$\Theta = \frac{1}{2}\left[\arctan(\Sigma) - \frac{\Sigma}{\Sigma^2+1} - \arctan(\Sigma_0) + \frac{\Sigma_0}{\Sigma_0^2+1}\right] \tag{16}$$

which is plotted in Figure 3. We find that sag advances similarly for small initial sheet curvatures $\sum_0 \leq 0.2$, but then

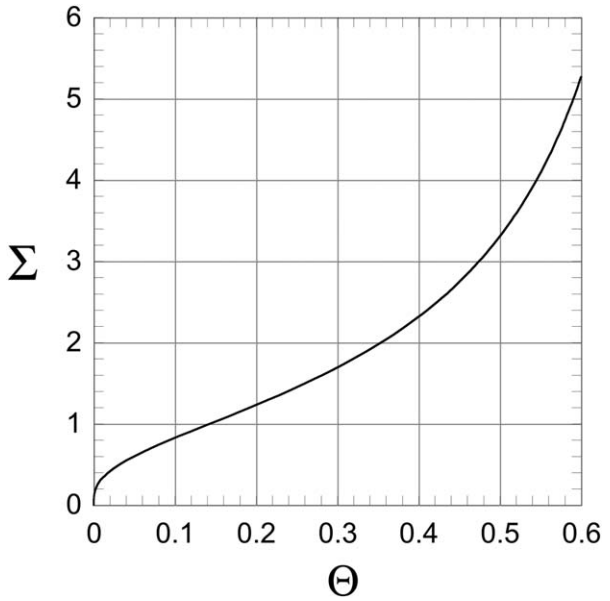

Figure 2. Analytical solution for dimensionless sag, $\sum$ vs. dimensionless time, Θ, for a Newtonian isothermal rectangular sheet pinned at just two edges but with an infinite length and with no initial sheet curvature [$\sum_0 = 0$] (Eq. 15).

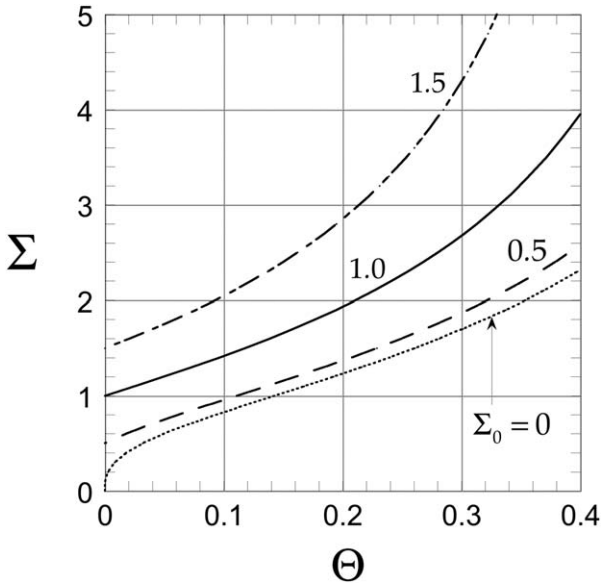

Figure 3. Analytical solution for dimensionless sag, $\sum$, vs. dimensionless time Θ, for a Newtonian isothermal rectangular sheet pinned at just two edges but with an infinite length and with initial sheet curvatures ($\sum_0 = 0, 0.5, 1.0, 1.5$).

eventually accelerates with the initial sheet curvature. We can account for initial droop using Eq. 16. In practice, the initial droop $\sum_0$ is much smaller than the final value of $\sum$. For instance, in our experiments (see the section Experimental Measurement of Commercial Sag) we measure an average droop of 0.75 in. for 36 × 73 in. HIPS sheets for a final value of sag of 4.75 in. Hence, in this work we focus our attention on the special of case of zero initial sheet curvature.

Parallel Superposition for Sheet Sag

We combine Eq. 15 with

$$\frac{1}{d_t} = \frac{1}{d_w} + \frac{1}{d_\ell} \tag{17}$$

which we call the *parallel superposition principle*, and which we use to calculate the amount of sag for a Newtonian isothermal sheet pinned all the way. We apply Eq. 15 twice, first to calculate the dimensional sag in the width direction d_w (Figure 4) and then in the length direction d_ℓ (Figure 5). Then Eq. 17 allows us to combine d_w and d_ℓ to

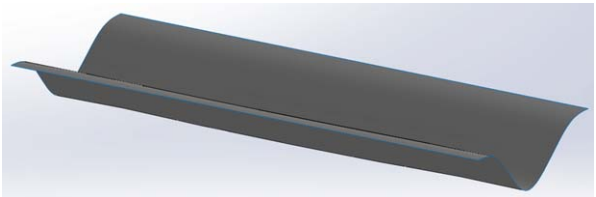

Figure 4. Sketch of a 36-in. width HIPS sheet sagging through its width, and pinned along its edges over its entire length (sample A of Table 4 and Eq. 15).

[Color figure can be viewed in the online issue, which is available at wileyonlinelibrary.com.]

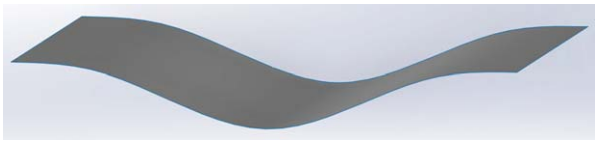

Figure 5. Sketch of a 73-in. long HIPS sheet sagging through its length and pinned along its ends over its entire width (sample A of Table 4 and Eq. 15).

[Color figure can be viewed in the online issue, which is available at wileyonlinelibrary.com.]

calculate the sag of a Newtonian isothermal sheet pinned all the way around d_t (Figure 6).

Experimental Measurement of Commercial Sag

In this study, we compare analytical solution, Eq. 15 combined with (17), to sag data for rectangular high-impact polystyrene (HIPS) sheets of various dimensions and approximately 2.5 mm average sheet thickness that we measured under commercial operating conditions. Table 4 lists the dimensions of these HIPS sheets. The third column of Table 4 lists the orientation of each sheet's extrusion direction (machine or transverse) with respect to the pinned edges in each of our sag experiments. Figure 7 shows sample A of Table 4, pinned all the way around, in the commercial thermoformer. The commercial thermoformer employed here incorporates a bank of ceramic (model MAAC-4, MAAC Machinery Corp., Carol Stream, IL) radiative heaters 7 in. above and 18 in. below the sheet. The bank dimensions were 62 × 108 in., and set to 700°F along its edges and 400–500°F at its center. The HIPS sheets were pinned all the way around. The sag values were then measured using a complementary metal-oxide semiconductor (CMOS) laser displacement sensor (model IL-600, Keyence, Osaka, Japan). Sheet temperatures were measured using MI3 infrared sensors (Raytek®, Santa Cruz, CA).

Results: Analytical vs. Measurements

We compare our analytical solution for a Newtonian isothermal sagging sheet pinned all the way around to commercial experimental measurements. Neglecting initial sheet curvature, we combine Eq. 15 with 17 to fit the sag measurements of sample A of Table 4. In Figure 8, we plot the sheet sag d_w, of an infinitely long sheet that has a finite width, 36 in., and the sheet sag d_l, of an infinitely wide sheet that has a finite length, 73 in., and we superpose them using Eq. 17 to plot the sheet sag of the HIPS sheet pinned all the way around d_t. We first fit the shape of the experimental measurements for sample A of Table 4 with the isothermal analytical solution to get a Newtonian viscosity value of

Figure 6. Sketch of a sagging 36×73 in. HIPS sheet pinned all the way around (sample A of Table 4).

[Color figure can be viewed in the online issue, which is available at wileyonlinelibrary.com.]

Table 4. Dimensions of HIPS Sheets used in Experiment

Sample	Dimension (in.)	Orientation direction (machine or transverse)	μ_s(Pa · s)
A	36 x 73	Machine	1.01×10^5
B	33 x 48	Machine	1.01×10^5
C	42 x 75	machine	9.1×10^4

Legend: Machine ≡ extruded along the sheet's longest dimension; transverse ≡ extruded along the sheet's shortest dimension.

1.01×10^5Pa · s. Then we fit the magnitude of the experimentally measured sheet sag $d_{\exp}$, using

$$d_{\exp} = d_t \zeta^{-1} \tag{18}$$

where we call ζ the *sag fitting parameter*. Here we find $\zeta=14$ for Samples A, B, and C of Table 4. Thus, we find that the isothermal theory sags 14 times faster than the nonisothermal commercial experiment, although we find that the time evolution of the commercial sag follows nearly exactly the same shape as the isothermal prediction. Similarly in Figure 9, HIPS sheets of different dimensions are also fitted using Eqs. 15, 17 and 18 to give Newtonian viscosities of 1.01×10^5Pa · s for Sample B and for 9.1×10^4Pa · s Sample C of Table 4. This is a simple method that uses our isothermal theory to fit sag measurements in commercial thermoforming, and also deduces the Newtonian viscosity of a sagging sheet above its softening point.

Finite Element Calculation of Sheet Sag

Here we calculate the sheet sag using the finite element method (FEM) with commercial software called ANSYS Polyflow version 14.5.[15,16] This software employs the numerical methods developed by Crochet at Université Catholique de Louvain in Belgium.[17] With this code, we simulate (1) a 2-D Newtonian isothermal sheet that is symmetric along the infinite sheet length, and we also simulate (2) a 3-D rectangular sheet pinned all the way around. Figure 10 shows the ANSYS Polyflow mesh of a rectangular HIPS sheet pinned at just two edges (case 1). Figure 11 is a 3-D mesh of a quarter sheet pinned all the way around (case 2).

Results: Finite Element Method (FEM)

Evaluation of analytical solution

Using ANSYS polyflow, we simulate a 2-D representation of an infinitely long, isothermal sagging sheet pinned at just two edges, that is, symmetric along its length, illustrated in Figure 10. In Figure 12, we show a good agreement between

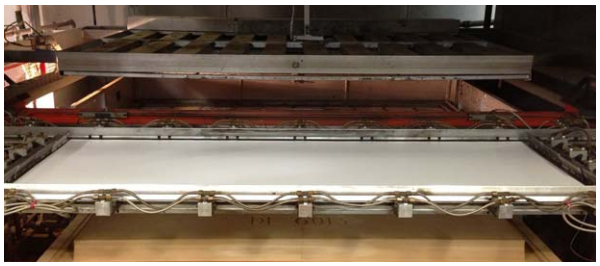

Figure 7. Experimental setup of 36×73 in. HIPS sheet pinned all the way around (sample A of Table 4).

[Color figure can be viewed in the online issue, which is available at wileyonlinelibrary.com.]

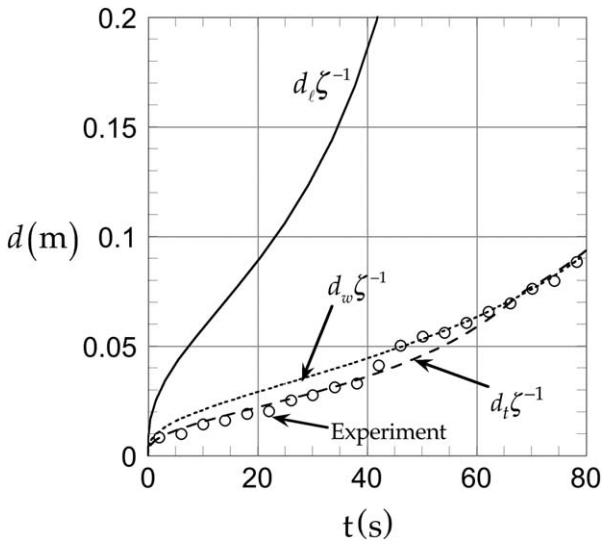

Figure 8. Analytical solutions (solid, dotted, and dashed curves) with $\mu_s = 1.01\times10^5$ Pa·s and a sag fitting parameter $\zeta = 14$, to fit the experimental measurements (circles) for a 36×73 in. HIPS sheet pinned all the way around.

The solid and dashed curves use Eq. 15 without superposition, and the dashed curve combines Eq. 15 with superposition, Eq. 17.

the dimensionless sag vs. dimensionless time for the analytical solution, Eq. 15, and FEM calculation for $\Sigma \leq \frac{3}{2}$.

Parallel superposition (effect of free edges)

Here we compare the analytical solution, Eq. 15 combined with 17 to FEM calculation for a HIPS sheet pinned all the way around, illustrated in Figure 11. In Figure 13, we show good agreement between the analytical solution (Eqs. 15

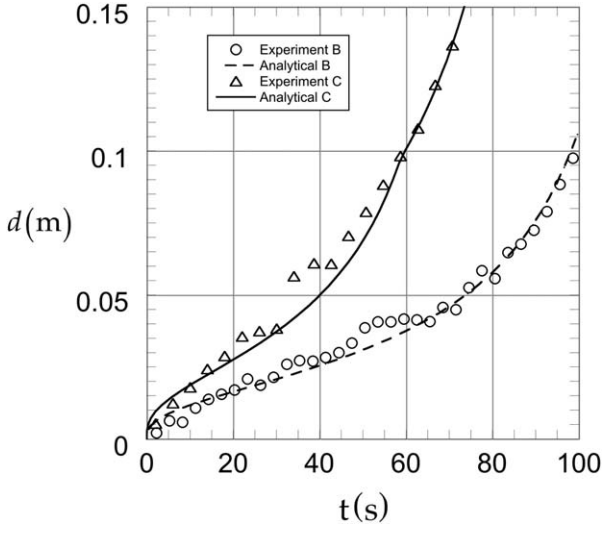

Figure 9. Additional measurements fitted with analytical solutions (Eq. 15 combined with superposition Eq. 17).

33 × 48 in. (dashed curve, $\mu_s = 1.01\times10^5$ Pa·s, ζ=14) and 42 × 75 in. (solid curve, $\mu_s = 9.1\times10^4$ P·s, ζ=14) HIPS sheets pinned all the way around.

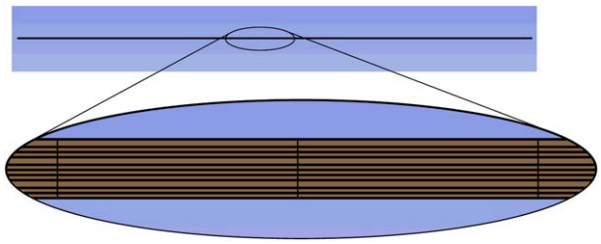

Figure 10. ANSYS Polyflow finite element mesh of an infinitely long sheet pinned at just two edges with a finite width.

Ten elements through the sheet thickness and 100 elements along its width. [Color figure can be viewed in the online issue, which is available at wileyonlinelibrary.com.]

and 17) and FEM calculation. Again we find that the cylindricity assumption is reliable when for $\Sigma \leq \frac{3}{2}$.

Sagometry

Thermoforming involves deformation of the softened sheet at a temperature that is just above the polymer softening point. Giacomin et al.[11] points out that the plastic sample near the softening point often tend to slip on the rheometer disk and the sample's free edges are prone to distort from their ideal nearly cylindrical shape. This makes measuring the plastic's softening viscosity using a parallel disk rheometer challenging. Following Giacomin et al.[11] we use Eq. 15 and Table 3 to give the Newtonian resin viscosity above the softening point of the plastic sheet μ_s

$$\mu_s \equiv \frac{\rho g r_0}{8\Theta} t \equiv \frac{\rho g r_0 t}{4\left[\arctan(\Sigma) - \frac{\Sigma}{\Sigma^2+1}\right]} \tag{19}$$

where the subscript s, meaning at the softening point, has been added. When a flow field is useful for determining the viscosity, we call it *viscometric* and the cylindrical sag, illustrated in Figure 1, is a viscoetric flow field. Such a gravity-driven free-boundary flow for viscometry is called *sagometry*.[11] We use Eq. 19 to report the Newtonian viscosities of rectangular HIPS sheets of various dimensions in Table 4

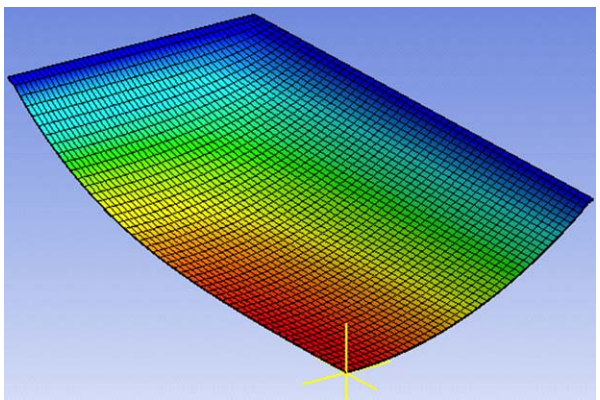

Figure 11. ANSYS Polyflow finite element mesh of a quarter sheet pinned all the way around.

Ten elements through the sheet thickness and 50 elements each along the sheet's length and width. [Color figure can be viewed in the online issue, which is available at wileyonlinelibrary.com.]

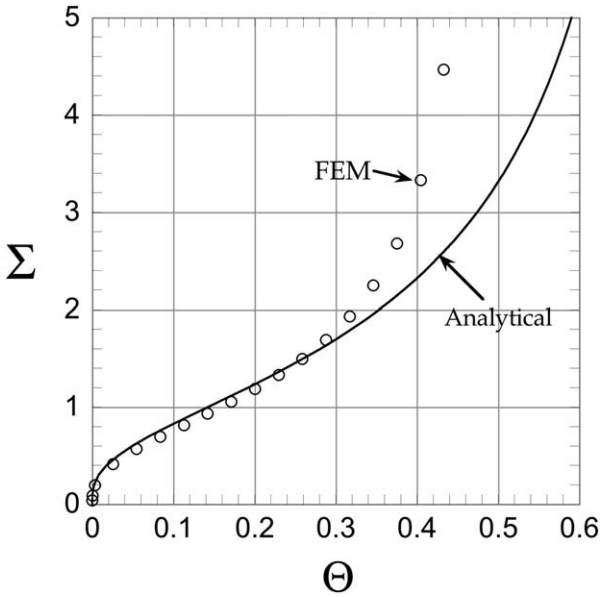

Figure 12. Dimensionless sag $\sum$ vs. dimensionless time Θ, for analytical solution (solid curve, Eq. 15 combined with superposition Eq. 17), and finite element calculation (circles, FEM) for a Newtonian isothermal sheet pinned at just two edges.

$r_0 = 36$ in. and $\mu_s = 1.01\times10^5$ Pa·s.

above their softening points. Eq. 19 can be used as the basis of a standardized testing for sag in thermoforming.

Conclusion

This analysis uses the approaches of Giacomin et al.[11] for their isothermal Newtonian case of sheet sag during thermoforming. We have successfully fitted the sag measurements in commercial thermoforming with our isothermal theory for a sheet pinned at just two edges, and employed the parallel

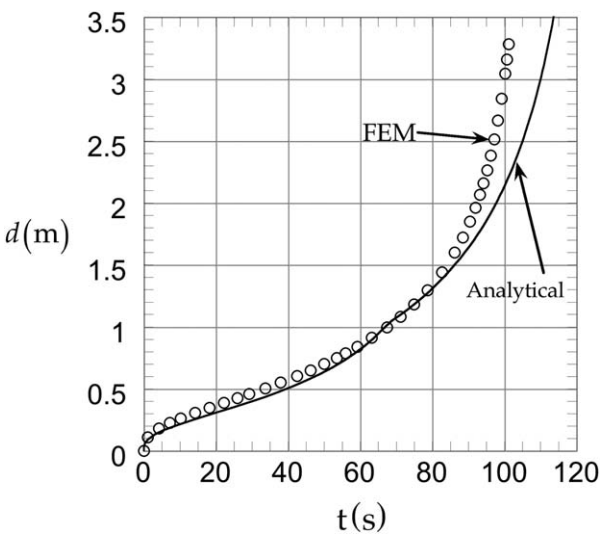

Figure 13. Analytical solution (Eq. 15 combined with superposition Eq. 17), and finite element calculation (circles, FEM) for a Newtonian, isothermal HIPS sheet with $\mu_s = 1.01\times10^5$ Pa·s pinned all the way around. The sheet dimensions are 36×73 in.

superposition principle for a sheet pinned all the way around. We find that the time evolution of the commercial sag follows nearly exactly the same shape as the isothermal prediction. From this we further discover that our isothermal theory overpredicts the experimental sag measurements by a sag fitting parameter ζ of 14 for the HIPS material. Accounting for recoil due to frozen-in stresses and sheet orientation would lower our prediction for sag below the value predicted by the isothermal prediction, Eq. 15. Also we have shown good agreement between our isothermal analytical solution and FEM calculations and found that our cylindricity assumption is reliable for $\Sigma \leq \frac{3}{2}$. Last, we have developed an equation to deduce the Newtonian viscosity of the sagging, rectangular HIPS sheet above its softening point by fitting experimental sag measurements to, within a factor, our isothermal analytical solution.

Acknowledgments

The authors acknowledge Sub-Zero, Inc. of Madison, WI, for its sponsorship. Also we are grateful of process operators and the entire team at Sub-Zero, Inc. for providing useful experimental measurements of sheet sag. We are indebted to ANSYS, Inc. of Canonsburg, PA for their University Partnership. We dedicate this article to Professor R. Byron Bird, Professor Emeritus of the University of Wisconsin-Madison, on the occasion of his ninetieth birthday (February 5, 2014).

Literature Cited

1. Michaud RA, Giacomin AJ. Sheet temperature in thermoforming. *J Plast Film Sheeting*. 2011;27(4):293–330.
2. Kershner MA, Giacomin AJ. Thermoforming cones. *J Plast Technol*. 2007:3;1–25.
3. Kershner MA. *Thermoforming Plastic Cups and Cones* [MS Thesis]. Mechanical Engineering Dept., University of Wisconsin, Madison, WI; 2007.
4. Lieg KL, Giacomin AJ. Thermoforming triangular trough. *Pol Eng Sci*. 2009;49;189–199.
5. Lieg KL. *Thermoforming Triangular Trough* [MS Thesis]. Mechanical Engineering Dept., University of Wisconsin, Madison, WI; 2008.
6. Baek HM, Giacomin AJ. Corotating or codeforming models for thermoforming. *J Adv Eng*. 2013;8(2):41–54.
7. Baek HM. *Corotating or Codeforming Rheological Models for Thermoforming* [MS Thesis]. Mechanical Engineering Dept., University of Wisconsin, Madison, WI; 2013.
8. Stephenson MJ. *An Experimental and Theoretical Study of Sheet Sag in the Thermoforming Process* [PhD Thesis]. State University of New York, Buffalo, NY; 1997.
9. Stephenson MJ, Dargush GF, Ryan ME. Application of one-dimensional mechanical formulations to model the sagging behavior of a polymer sheet. *Polym Eng Sci*. 1999;39:2199–2221.
10. Sentmanat ML. Miniature universal testing platform: from extensional melt rheology to solid-state deformation behavior. *Rheol Acta*. 2004;43:657–669.
11. Giacomin AJ, Mix AW, Mahmood O. Sag in thermoforming. *Polym Eng Sci*. 2010;50(10):2060–2068.
12. Bird RB, Stewart WE, Lightfoot EN. *Transport Phenomena*, revised 2nd ed. New York: John Wiley and Sons, Inc; 2007.
13. Bird RB, Armstrong RC, Hassager O, *Dynamics of Polymeric Liquids*. vol. 1. Fluid Mechanics, 2nd ed. New York: Wiley & Sons; 1987.
14. Nair B, Track measurement systems-concepts and techniques. *Rail Int*. 1972;3(3):159–166.
15. ANSYS Polyflow Version 14.5, ANSYS, Inc., Canonsburg, PA; 2012.
16. ANSYS Polyflow Version 14.5 User's Guide. ANSYS, Inc., Canonsburg, PA; 2012.
17. Van Schaftingen JJ, Crochet MJ. A comparison of mixed methods for solving the flow of a Maxwell fluid. *Int J Numerical Methods Fluids*. 1984;4:1065–1081.
18. Cruz CA. Rheology of acrylic-modified polypropylene for thermoforming. Polyolefin VIII, SPE RETECH, Proceedings, Houston, TX; Feb 21–24; 2012:523–538.
19. Lucas BM, Krishnamurthy V, Bonser JR. Propylene compositions with improved resistance to thermoforming sag. US Patent No. 5,439,949. August 8, 1995.
20. Stephenson MJ, Ryan ME. A study of the sagging of styrenic sheets associated with the thermoforming process. Annual Technical Conference Proceedings; Boston, MA; May 7–11; 1995:794–795.
21. Lau HC, Bhattacharya SN, Field GJ. Melt strength of polypropylene: Its relevance to thermoforming. *Polym Eng Sci*. 1998;38(11):1915–1923.
22. Lau HC, Bhattacharya SN, Field GJ. Influence of rheological properties on the sagging of polypropylene and ABS sheet for thermoforming applications. *Polym Eng Sci*. 2000;40(7):1564–1570.
23. Duarte FM, Covas JA. IR sheet heating in roll fed thermoforming: Part 1 - Solving direct and inverse heating problems. *Plast Rubb Comp*. 2002;31(7):307–317.
24. Debergue P, Girard P, Grandpré C. Improving the prediction of thermoforming sag in simulations through experimental validation of the transition model. Annual Technical Conference Proceedings; Chicago, IL; May 16–20, 2004:914–918.
25. Gupta AV, Misra D. Behavior of polymer sheet during sagging phase. *Int SAMPE Symp Exhib Proc*. 2006;51:14.
26. Mohammadiain-Gezaz S, Ghasemi I, Azizi H, Karrabi M. Influence of the β-nucleator on the thermal and sagging behaviours of polypropylene. *Iran Polym J*. 2006;15(8):637–644.
27. Baek HM, Giacomin AJ, Wurz MJ. Sag in commercial thermoforming: Analytical solution versus finite element calculation. Abstracts, 2013 ANSYS Regional Conference; Detroit, Convergence, Detroit, MI; June 4, 2013:3.

Manuscript received July 16, 2013, and revision received Sept. 27, 2013.